NJC

ROYAL SOCIETY OF CHEMISTRY

PAPER

View Article Online
View Journal

Cite this: DOI: 10.1039/d4nj03697b

Crystal chemistry and luminescence properties of tetrabutylphosphonium tetrakis(8-quinolinato)-lanthanidate $[P_{4444}][Ln(Q)_4]\cdot 2X$ (X = H_2O and $(CH_3)_2CO$)

Stefanie Kammereck,[a] Guillaume Bousrez,[ab] Olivier Renier,[a] Veronica Paterlini,[a] Volodymyr Smetana[ab] and Anja-Verena Mudring *[abcd]

Since the discovery of AlQ_3 (Q = 8-quinolinolato) quinolinato complexes, they have been extensively scrutinized as emitter materials for organic lighting. Herein, we report on the first representatives of a series of tetrabutylphosphonium tetrakis(8-quinolinolato)lanthanidate complexes $[P_{4444}][Ln(Q)_4]\cdot 2X$ (Ln = Dy–Lu and Y; X = H_2O for Ln = Dy–Tm, Lu and Y and $(CH_3)_2CO$ for Ln = Yb), which are synthesised by a simple metathesis reaction of the respective potassium tetrakis(8-quinolinolato)lanthanidate salts with tetrabutylphosphonium bromide in acetone at room temperature. Single-crystal X-ray diffraction reveals that Ln(III) is coordinated by four bidentate 8-quinolinato ligands in the form of a distorted square antiprism. The distinct $[Ln(Q)_4]^-$ anions interact with the $[P_{4444}]^+$ cations through secondary bonding interactions, such as CH–π and van der Waals interactions, in addition to electrostatic coulombic interactions. Although these compounds contain crystal water/solvent molecules (and their synthesis does not require an inert atmosphere), they do not enter the metal coordination sphere but form pairwise intramolecular hydrogen bonds with the two 8-quinolinato ligands of the complex lanthanide anions. Combined differential scanning calorimetry–thermogravimetric analysis indicates that crystal water is lost at around 100 °C and $[P_{4444}][Ln(Q)_4]$ is formed, which is stable up to 300 °C, where further degradation occurs. All compounds feature strong emission in the green region, originating from the π* → π transitions within the 8-quinolinato ligand, with lifetimes in the nanosecond range. The luminescence colour changes from blue-green to yellow-green depending on Ln^{3+}, which opens up additional directions in the colour tuning of emitters for organic lighting applications.

Received 22nd August 2024,
Accepted 6th August 2025

DOI: 10.1039/d4nj03697b

rsc.li/njc

Introduction

Efficient and readily accessible materials for optical applications such as solid state lighting are particularly important for guaranteeing a high standard of living in a sustainable society.[1] For this reason, coordination compounds with chelating ligands are garnering strong interest.[2] In particular, since the discovery of tris(8-quinolinato)aluminium (AlQ_3),[3,4] as an efficient OLED (organic light emitting device)[5] emitter, the 8-hydroxyquinolinato (Q) ligand and its derivatives have attracted attention as ligands.[6,7] The photoluminescence quantum yield of 8-hydroxyquinoline (HQ) is very low because of rapid proton-exchange and vibrational quenching.[8] This problem can be mitigated through organisation in a rigid network, either as a cation[9] or *via* deprotonation and coordination to a metal cation, as in AlQ_3. In the context of application as emitter materials, lanthanide compounds offer a broader range of accessible photophysical properties owing to their partially filled 4f orbitals, enabling the fine-tuning of luminescence. Moreover, trivalent lanthanide ions often form more robust coordination frameworks than Al^{3+}, which is advantageous because it helps suppress vibrational quenching and is particularly valuable for near-infrared applications. Similar to aluminium, the most stable oxidation number for most lanthanides is +III. Therefore, it was speculated that isostructural compounds would form.[10,11] However, structural analysis shows that LnQ_3 instead forms multinuclear, trimeric units $[Ln_3Q_9]$ while occasionally incorporating non-coordinating solvent molecules.[12–17] Interestingly, despite the strong interest in Ln complexes with 8-quinolinato (Q), reports on the structural data of homoleptic compounds are scarce. However, the exclusion of water and other molecules from the immediate coordination

[a] Department of Materials and Environmental Chemistry, Stockholm University, Svante Arrhenius väg 16C, 10691 Stockholm, Sweden
[b] Department of Biological and Chemical Engineering & iNANO, Aarhus University, 8000 Aarhus C, Denmark. E-mail: anja-verena.mudring@bce.au.dk
[c] Department of Physics, Fysikhuset, Umeå University, Linnaeus väg 24, 901 87 Umeå, Sweden. E-mail: anja-verena.mudring@umu.se
[d] University of KwaZulu-Natal, Howard College Campus, Durban 4041, South Africa

sphere of Ln(III) is important as it is a source of vibrational quenching, particularly for neodymium(III), erbium(III), and ytterbium(III), which can serve as near-infrared emitter materials.[18–21] Reports on the structure of LnQ_3 and the formation of homoleptic lanthanide quinolinolates $[AMLnQ_4]$ upon reaction with alkali metal quinolinolate (AM = alkali metal) in a flux of 1,2,4,5-tetramethylbenzene[22] motivated us to explore whether homoleptic quinolinolato complex anions of lanthanides could be accessible through conventional solution chemistry. To ensure the exclusion of water from the lanthanide coordination sphere, we chose hydrophobic tetraalkylphosphonium cations instead of alkali metal cations under ambient conditions. In the light of potential applications in organic lighting, the general properties of phosphonium countercations for $[Ln(Q)_4]^-$, such as comparatively high thermal and electrochemical stability, are attractive, particularly when compared to ammonium analogues.[23–26] While experimentally exploring these systems and submitting our manuscript, a study on the use of 8-hydroxyquinolinato complexes for the separation of metals in NdFeB magnets through selective precipitation was published,[27] showing the additional use of these complexes.

Herein, we report the synthesis and structures of $[P_{4444}][Ln(Q)_4]\cdot 2H_2O$ (Ln = Dy–Tm, Lu and Y) and $[P_{4444}][Yb(Q)_4]\cdot 2(CH_3)_2CO$ together with the thermal and optical properties.

Results and discussion

Synthesis

$[P_{4444}][Ln(Q)_4]\cdot 2X$ (Ln = Dy–Lu and Y; Q = 8-quinolinolato; X = H_2O for Ln = Dy–Tm, Lu and Y and $(CH_3)_2CO$ for Ln = Yb) was synthesized by a metathesis reaction of the respective potassium tetrakis(8-quinolinolato)lanthanidate salts with tetrabutylphosphonium bromide in acetone at room temperature (Scheme 1).

$$[P_{4444}]Br + K[Ln(Q)_4] \xrightarrow[-\ KBr]{\text{Acetone}} [P_{4444}][Ln(Q)_4]\bullet 2X \quad (X = H_2O \text{ or } (CH_3)_2CO)$$

Scheme 1 General synthetic procedure for $[P_{4444}][Ln(Q)_4]\cdot 2H_2O$ (Ln = Dy–Lu, Y) and $[P_{4444}][Yb(Q)_4]\cdot 2(CH_3)_2CO$.

Structure analysis

Transparent, slightly yellow-coloured needle-shaped crystals of $[P_{4444}][Ln(Q)_4]\cdot 2H_2O$ (Ln = Dy–Tm, Lu and Y) and $[P_{4444}][Yb(Q)_4]\cdot 2(CH_3)_2CO$ of sufficient quality for single X-ray structure analysis (SCXRD) were obtained by slowing the isothermal evaporation of the acetone solutions. Interestingly, reactions with lanthanides larger than Dy were not successful, and only X-ray amorphous precipitates were formed. Structural analysis of all compounds revealed that the asymmetric unit is composed of one $[Ln(Q)_4]^-$ anion complemented by two H_2O or acetone molecules and charge-balanced by one $[P_{4444}]^+$ cation. The structure $[P_{4444}][Ln(Q)_4]\cdot 2H_2O$, Ln = Dy, is discussed as a representative of the isostructural series of hydrates (see also Fig. S1–S8). The lanthanide(III) ion coordinates with four bidentate 8-hydroxyquinolinato ligands in the form of a slightly distorted square antiprism (Fig. 1(a)). The ONO and NON angles of the prism bases are in the ranges of 74.3–79.8(1)° and 99.9–105.2(1)°, respectively, while the N–O edges are 2.689–3.093(7) Å. Each ligand coordinates both through its N atom at the pyridine ring and the O atom of the phenolic moiety, which is a commonly observed coordination mode in metal quinolinates, such as $B[Ln(Q)_4]$ or $B[Ln(Q)_4]\cdot xH_2O$ (B = monovalent cation, Li^+, Na^+, K^+, Rb^+ or NH_4^+).[22,26] The ligands are oriented around the central metal cation, resembling a projected X (Fig. 1(a)). The interatomic Dy–O and Dy–N contacts show a narrow distribution with values of 2.276–2.293(5) Å and 2.526–2.595(5) Å, which are in the expected range.[26] The O-atoms of each 8-quinolinato ligand further bind pairwise to a water molecule with rather moderate OH···O hydrogen bonds (d_{O-O} = 2.86–2.98(1) Å) (Fig. 1(b)).

The distorted PC_4 tetrahedron in the $[P_{4444}]^+$ cation is characterized by CPC angles in the range of 102.8–116.7(6)°. The butyl chains exhibit two different shapes (linear and hook) with CCCC torsion angles in the 137–175(1)° range for the former and 57(1)° for the latter. It is also noteworthy that a decent

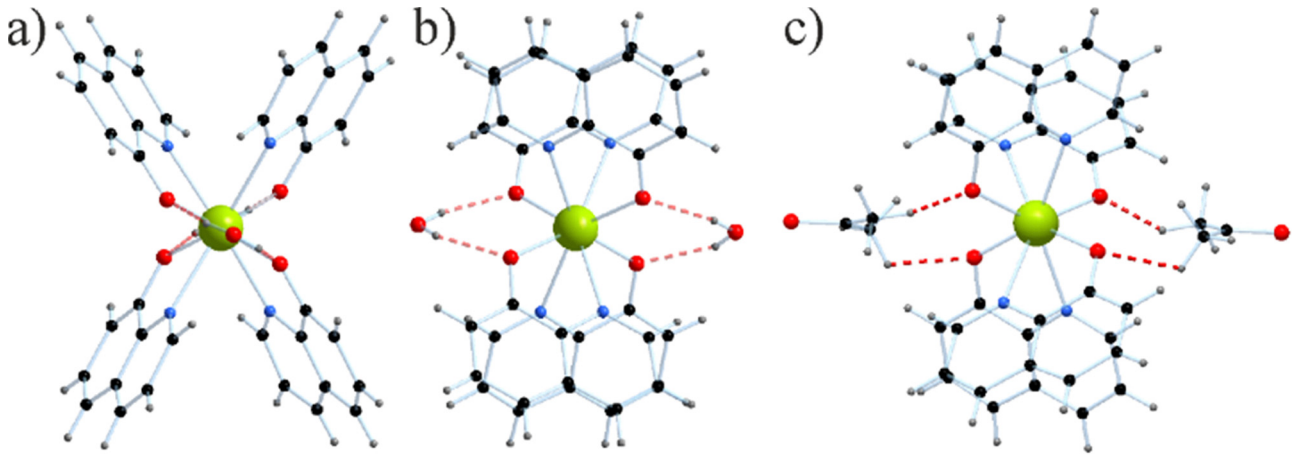

Fig. 1 Molecular structures of $[Dy(Q)_4]^-\cdot 2H_2O$ (a) and (b) and $[Yb(Q)_4]^-\cdot 2(CH_3)_2CO$ (c). Ln atoms are green, oxygen atoms are red, carbon atoms are black, nitrogen atoms are blue, and hydrogen atoms are grey in all figures.

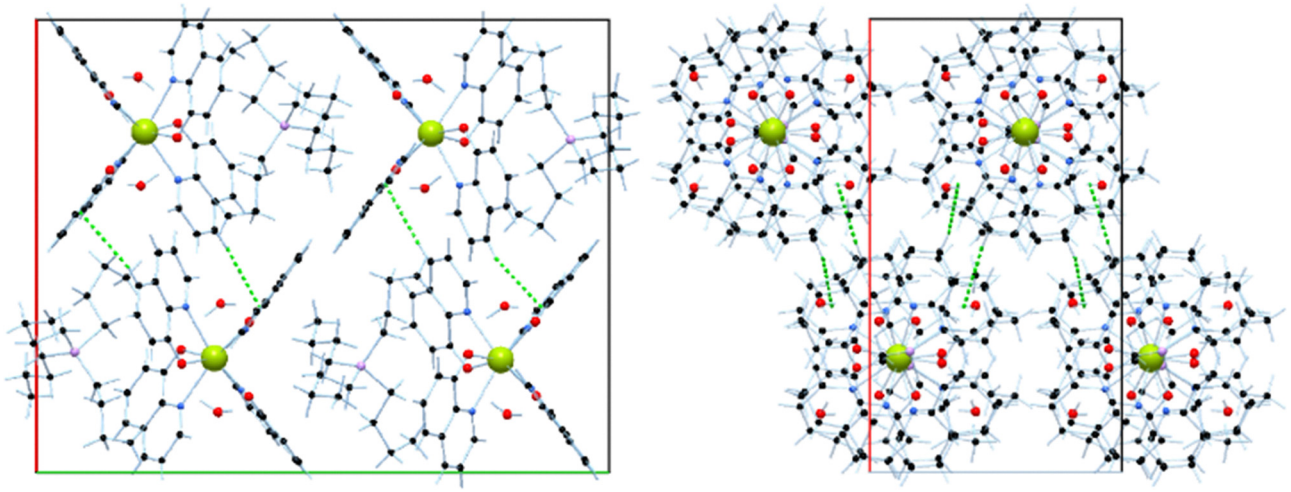

Fig. 2 Packing in the crystal structures of $[P_{4444}][Dy(Q)_4]\cdot 2H_2O$. Left: Projection along the crystallographic *c*-axis. Right: Projection along the crystallographic *b*-axis. Crystallographic axes are color coded: a – red, b – green, and c – blue.

disorder of the cation was observed in all the above structures involving two out of four butyl chains. The affected disordered chains represent mixtures of linear and hook conformations with proportions varying from ∼1 : 1 to ∼3 : 2 (Fig. S1).

The crystal packing of $[P_{4444}][Ln(Q)_4]\cdot 2H_2O$ (Fig. 2) is characterized by cations and anions alternating along the *b* axis, forming columns (Fig. 2, right). The X-shape of the complex anions allows for efficient packing of the cations along the *b* axis. Such columns stack hexagonally in the *ac* plane, exhibiting two types of weak interactions: –CH···π (along with the *ac* diagonals) and van der Waals (along with the *c* axis). The distances between the aromatic ring centroids are quite large (>4.5 Å). However, we can observe CH···π interactions (highlighted by green dashed lines) that can be considered weak bonding ($d_{Cg\cdots HC}$ = 2.88–3.01(1) Å). These interactions are responsible for connectivity along the *a* axis connecting the columns into a 3D framework.

When comparing the structure of $[P_{4444}][Yb(Q)_4]\cdot 2(CH_3)_2CO$ to $[P_{4444}][Ln(Q)_4]\cdot 2H_2O$ (Ln = Dy–Tm, Lu and Y), it is interesting to note that the substitution of water with acetone practically does not affect the local structure of the $[Ln(Q)_4]^-$ anion. Instead of water, the acetone CH_3 groups serve as H-bond donors, establishing bridges between the two 8-quinolinato ligands of a $[Ln(Q)_4]^-$ unit (Fig. 1(c)). Although the C(H)···O distances are relatively short (2.606–2.700(9) Å), these interactions are not directional. Similarly, Ln–O and Ln–N bonding appear to be largely unaffected. The interatomic distances decrease slightly for $[Yb(Q)_4]^-$ (2.225–2.253(5) for Ln–O and 2.485–2.527(5) Å for Ln–N) compared to $[Dy(Q)_4]^-$, which can be attributed to the lanthanide contraction, as can be derived from the ionic radii.[28] Despite the similar local environment, the bulkier nature of the acetone ligand leads to a rather significant packing rearrangement (Fig. 3). In the *ab* plane, we still observe an identical alternation of anions and cations along the −*ab* diagonal, forming columns. These columns in turn establish a dense network of CH···π contacts ($d_{Cg\cdots HC}$ = 2.65–3.02(1) Å) between the above and below lying columns (4 contacts per complex pair). In contrast to the previous complexes, these contacts did not branch, resulting in layers. The connectivity between the layers is established solely *via* weaker van der Waals interactions.

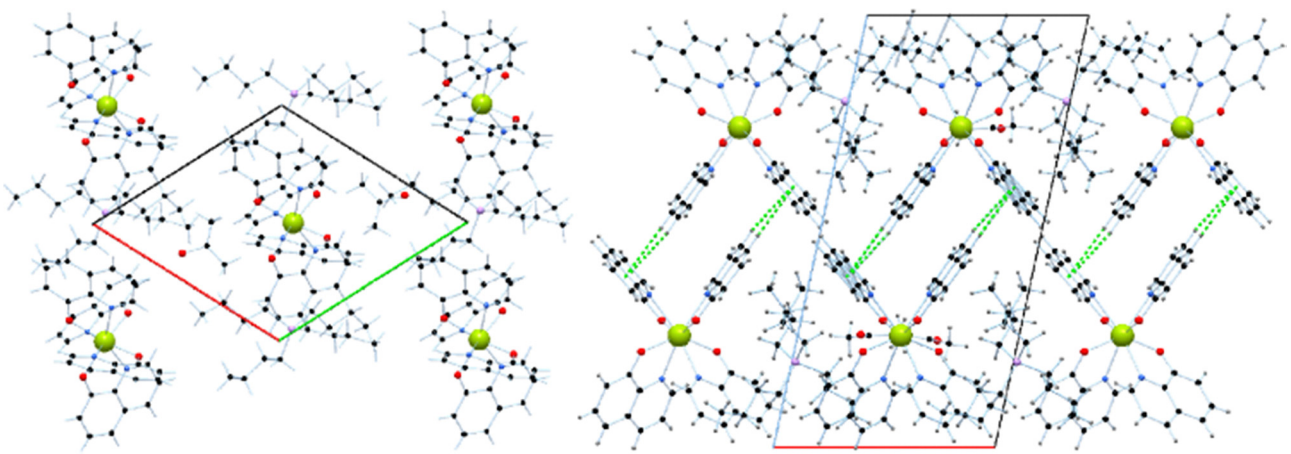

Fig. 3 Molecular packing in the crystal structure of $[P_{4444}][Yb(Q)_4]\cdot 2(CH_3)_2CO$.

Thermal analysis

Differential scanning calorimetry (DSC). The thermal behaviour of $[P_{4444}][Ln(Q)_4]\cdot 2H_2O$ (Ln = Dy–Tm, Lu and Y) was studied by differential scanning calorimetry (DSC) (Fig. S19). The traces are similar for all the complexes synthesized. Upon the first heating, a broad endothermic process was observed from 60 °C to 110 °C. This can be attributed to the loss of water molecules, as confirmed by thermogravimetric analysis (TGA, Fig. S20–S26). Upon cooling, no thermal events were recorded. Consequential heating and cooling cycles did not result in any thermal transition in the examined temperature range.

Thermogravimetry analysis

The thermal stability of the complexes was studied by thermogravimetry analysis (TGA) (Table S2 and Fig. S20–S26). The thermograms for all the compounds indicated two different steps of degradation. The first step occurs around 100 °C and corresponds to the loss of the two water molecules and formation of $[P_{4444}][Ln(Q)_4]$. The second step of the degradation process occurs between around 345 ± 5 °C for $[P_{4444}][Ln(Q)_4]\cdot 2H_2O$ (Ln = Dy–Tm, Lu) and slightly lower for $[P_{4444}][Ln(Y)_4]\cdot 2H_2O$ (Table 1). In this step, the compounds ($[P_{4444}][Ln(Q)_4]$) lose about 40% of the mass, which corresponds well to the loss of $[P_{4444}][Q]$ (40.3%), implying that LnQ_3 remains at the end of this decomposition step, whose decomposition can be observed at temperatures above 500 °C, after the measurement temperature.

Apart from the Y-compound, the decomposition occurs at lower temperatures with increasing Ln–O contact (considering also the different SXRD data collection temperatures) and decreasing Ln^{3+} radius (Table 1 and Table S1).

Luminescence study

The optical properties of all the compounds $[P_{4444}][Ln(Q)_4]\cdot 2H_2O$ (Ln = Dy–Tm, Lu and Y) are governed by the spectral features of the 8-quinolinato ligands. In the excitation spectra, these become apparent in the region of 280–450 nm (see Fig. S27), which originates from the π → π* transitions of the conjugated aromatic system of the 8-quinolinato anion, as observed for other metal quinolinates with optically inactive cations.[21,29–32] Correspondingly, all compounds feature an emission band in the green region (see CIE diagram Fig. 4, top) originating from the π* → π transition upon excitation of the respective transition (Fig. 4, bottom). The large Stokes shift between the excitation and emission wavelengths for the π → π* transition has already been observed for analogous compounds and has been attributed to fast structure relaxation after the excitation process.[33]

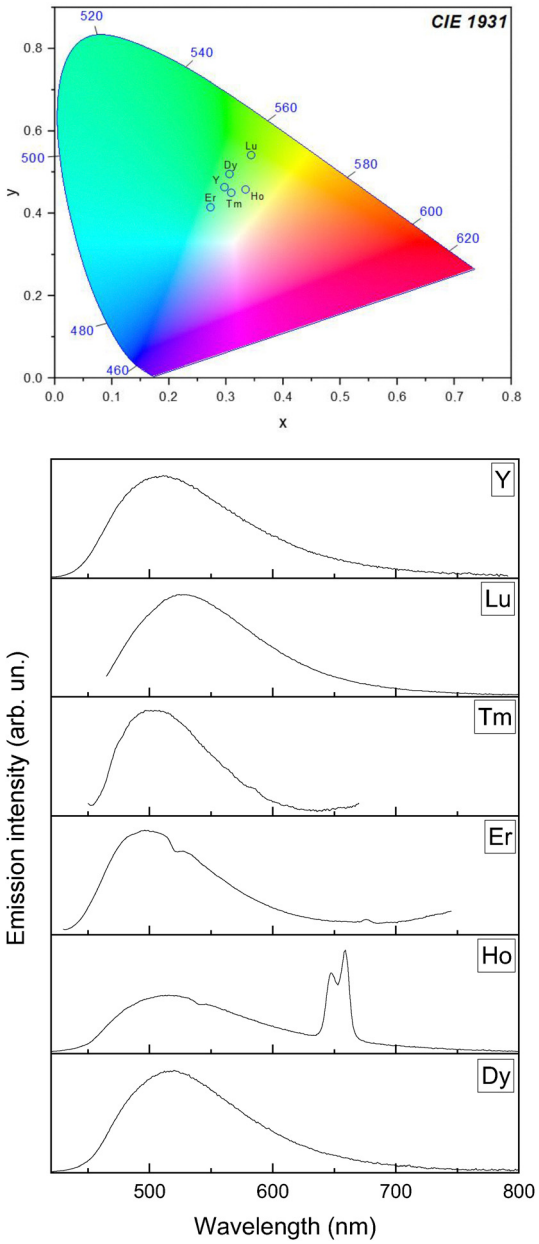

Fig. 4 CIE diagram (top) and emission spectra (bottom) for all the $[P_{4444}][Ln(Q)_4]\cdot 2H_2O$ complexes. The excitation wavelengths are 350 nm (Dy), 350 nm (Ho), 410 nm (Er), 430 nm (Tm), 436 nm (Lu) and 345 nm (Y).

Table 1 Decomposition temperature of $[P_{4444}][Ln(Q)_4]$ and interatomic distances in $[P_{4444}][Ln(Q)_4]\cdot 2H_2O$

	Decomposition temperature ($T_{5\%onset}$, °C)	Ln–O/Å	Ln–N/Å	Ln^{3+} (ionic radius for CN 8/Å)[28]
$[P_{4444}][Dy(Q)_4]$	347	2.282–2.291(8)	2.521–2.603(9)	Dy (1.027)
$[P_{4444}][Ho(Q)_4]$	349	2.273–2.282(7)	2.517–2.604(8)	Ho (1.015)
$[P_{4444}][Er(Q)_4]$	342	2.257–2.292(9)	2.524–2.590(9)	Er (1.004)
$[P_{4444}][Tm(Q)_4]$	339	2.250–2.262(8)	2.494–2.566(8)	Tm (0.994)
$[P_{4444}][Lu(Q)_4]$	340	2.233–2.248(6)	2.486–2.560(7)	Lu (0.977)
$[P_{4444}][Y(Q)_4]$	320	2.269–2.284(5)	2.531–2.579(6)	Y (1.019)

Table 2 Lifetime of complexes $[P_{4444}][Ln(Q)_4]$

	Ln	Lifetime (ns)	Ln–O/Å	Ln–N/Å	Ln^{3+} (ionic radius for CN 8/Å)[27]
$[P_{4444}][Dy(Q)_4]$	Dy	8	2.282–2.291(8)	2.521–2.603(9)	Dy (1.027)
$[P_{4444}][Ho(Q)_4]$	Ho	4	2.273–2.282(7)	2.517–2.604(8)	Ho (1.015)
$[P_{4444}][Er(Q)_4]$	Er	∼3	2.257–2.292(9)	2.524–2.590(9)	Er (1.004)
$[P_{4444}][Tm(Q)_4]$	Tm	<3	2.250–2.262(8)	2.494–2.566(8)	Tm (0.994)
$[P_{4444}][Lu(Q)_4]$	Lu	∼3	2.233–2.248(6)	2.486–2.560(7)	Lu (0.977)
$[P_{4444}][Y(Q)_4]$	Y	12	2.269–2.284(5)	2.531–2.579(6)	Y (1.019)

Electronically, the emission transition corresponds to a $\pi^* \rightarrow \pi$ charge distribution from the phenolic ring, where the HOMO (highest molecular orbital) to the pyridyl ring and the LUMO (lowest unoccupied molecular orbital) resides in Q.[34] It has been reported that increasing covalency in the metal–ligand bond (which is predominantly formed through metal–N interactions) leads to a red-shift in emission, while an increasing ionicity results in a blue-shift.[35] Consequently, it is expected that the luminescence properties of $[P_{4444}][Ln(Q)_4]\cdot 2H_2O$ (Ln = Dy–Tm, Lu and Y) are influenced by the metal–Q interactions. We observed herein that an increased metal–Q interaction, as evidenced by shorter Ln–O and Ln–N contacts (Table 2), leads to a decrease in the HOMO–LUMO gap, confirmed by the red-shift observed in the emission spectra (Fig. 4, bottom). However, as mentioned before, the complex formation prevents proton transfer, which is a prominent quenching mechanism observed for the protonated ligand, the neutral HQ.[30] In addition, the coordination of Q to a metal centre improves structural rigidity, significantly decreasing the probability of non-radiative transitions. Recorded luminescence lifetimes are 8 ns for $[P_{4444}][Dy(Q)_4]\cdot 2H_2O$, 4 ns for $[P_{4444}][Ho(Q)_4]\cdot 2H_2O$ and 12 ns for $[P_{4444}][Y(Q)_4]\cdot 2H_2O$. For $[P_{4444}][Er(Q)_4]\cdot 2H_2O$ and $[P_{4444}][Lu(Q)_4]\cdot 2H_2O$, the lifetime was very close to the instrument detection limit and estimated to be around 3 ns, while it was even shorter and not measurable for $[P_{4444}][Tm(Q)_4]\cdot 2H_2O$. Thus, with shorter Ln–Q contacts, the luminescence lifetimes become shorter, indicating increasing radiationless decay through vibrational quenching.

Among the investigated Ln^{3+}, only Dy and Ho feature emissions in the visible region of light. In particular, the main transition of Dy^{3+}, $^4F_{9/2} \rightarrow {}^6H_{13/2}$, occurs at 570 nm (approximately 19 230 cm^{-1}), while the main transition of Ho^{3+}, $^5S_2 \rightarrow {}^5I_8$, is expected to occur at 550 nm (approximately 18 180 cm^{-1}).[35] These lines both overlap with the emission band of the ligand, with a low difference in energy between the expected Ln^{3+} transition and the maximum of the observed emission from the Q ligand (1687 cm^{-1} for $[P_{4444}][Dy(Q)_4]\cdot 2H_2O$ and 1236 cm^{-1} for $[P_{4444}][Ho(Q)_4]\cdot 2H_2O$). This proximity renders an energy back transfer from the metal to the ligand extremely likely: the deactivation of the Ln^{3+} level is not a radiative emission to the ground level of Ln^{3+}, but it is absorbed by the Q levels, in a way that the emission spectrum mostly originates by the following emission by the ligand level and not by the characteristic transitions of the Ln^{3+}. This can explain why Q emission is predominant and is the only band that appears in the spectrum of $[P_{4444}][Dy(Q)_4]\cdot 2H_2O$ (Fig. 4, bottom). However, the $^5F_2 \rightarrow {}^5I_8$ transition of Ho^{3+} is quite strong and is located at the edge of the ligand emission band and around 3900 cm^{-1} lower than the maximum of the ligand band, so two peaks are visible in the spectra at 648 and 659 nm, attributable to this transition according to the Dieke diagram (Fig. 4, bottom).[36] This assignment is confirmed by the presence of two weak peaks at 479 and 489 nm in the corresponding excitation spectra (see Fig. S28), attributable to the $^5I_8 \rightarrow {}^5F_3$ transition.[37] The lifetime of $[P_{4444}][Dy(Q)_4]\cdot 2H_2O$ was also acquired upon excitation at different wavelengths, corresponding to the maximum expected for Dy^{3+} emission (570 nm) and to several other points of the 8-quinolinato emission band. The results (see Fig. S29) show that the longer decay is obtained in the range of the Dy $^4F_{9/2} \rightarrow {}^6H_{13/2}$ transition. Even though the decay is only slightly longer than the lifetime corresponding to the maximum of the Q band, this suggests the presence of a different emitting species. The lifetime in the nanosecond region can be due to an inefficient energy transfer or to a high deactivation rate of the radiative emission of the lanthanide. Moreover, a more efficient energy transfer from the ligand to Ho compared to the Dy sample can be assumed from the (slightly) closer proximity of Ho to the ligand, as confirmed by the shorter Ho–N (*i.e.*, on average, ⟨2.549 Å⟩ for Ho–N compared to ⟨2.562 Å⟩ for the Dy–N) and Ho–O distances as well as the overall smaller volume of the unit cell for $[P_{4444}][Ho(Q)_4]\cdot 2H_2O$ sample (4830.7 $Å^3$) than $[P_{4444}][Dy(Q)_4]\cdot 2H_2O$ (4872.2 $Å^3$).

Experimental

Materials and methods

Chemicals. Tributylphosphine (97%), 1-bromobutane, 8-hydroxyquinoline and potassium hydroxide were purchased from Sigma-Aldrich (Merck, Steinheim, Germany). Lanthanide chloride hydrates were obtained from the reaction between Ln_2O_3 (HEFA Rare Earth Canada Co. Ltd, Richmond, British Columbia, Canada) and HCl (37%, VWR Chemicals, Fontenay-sous-Bois, France). All solvents were 'solvent grade' and used as received without additional purification.

SCXRD. The main paragraph of the text follows directly here. Data for single crystal X-ray diffraction (SCXRD) analysis were recorded using a Bruker D8 Venture (MoKα, at 100 K) (Bruker AXS, Karlsruhe, Germany). Crystal structure solution by intrinsic phasing using SHELXT[38] yielded the preliminary structure solution in the space group $Pna2_1$ for $[P_{4444}][Ln(Q)_4]\cdot 2H_2O$ with Ln = Dy–Lu. Refinement with SHELXL[39] allowed for the

location and proper assignment of the remaining atom positions. The consequent solution in the centrosymmetric space group *Pccn* not only resulted in significantly higher R values but also significantly increased the degree of disorder involving all butyl chains and aromatic rings. However, the higher symmetry could not support reasonable modelling of the disordered components. Although heavy atoms emulate centrosymmetric structures, light atoms destroy them. The structure of $[P_{4444}][Yb(Q)_4]\cdot 2(CH_3)_2CO$ was refined in space group $P\bar{1}$, and SQUEEZE software was applied for the proper interpretation of the disordered solvent that could not be modelled. Hydrogen atoms were added and treated with the riding atom mode. Data reduction was performed with the program package X-Red or SAINT, and absorption corrections were carried out with the programs X-Shape or SADABS.[40,41] To illustrate the crystal structures, the programs Diamond and Mercury were used.[42,43]

PXRD. Powder X-ray diffraction (PXRD) data were recorded at ambient temperature using a PANalytical X'pert PRO diffractometer (Malvern Panalytical, Malvern, United Kingdom) with CuKα1 radiation on powder samples dispersed on a zero-background silicon wafer. The data were recorded in reflection mode from 5° to 70°, with a step size of 0.01° for 60 min at 0.55 s per step.

NMR. ^{1}H- and ^{13}C-NMR (nuclear magnetic resonance) spectra (Fig. S9–S18) were recorded at room temperature in DMSO-d_6 using a Bruker 400 MHz spectrometer equipped with a BBO probe (Bruker AXS, Karlsruhe, Germany). Chemical shifts are reported in delta (δ) units, expressed in parts per million (ppm). The following abbreviations are used for the observed multiplicities: d (doublet), t (triplet), dd (double doublet), and m (multiplet, for unresolved lines). ^{1}H-NMR chemical shifts were referenced to the residual solvent signal for DMSO (2.50 ppm), and ^{13}C-NMR chemical shifts were referenced to the solvent signal of DMSO (39.52 ppm).

Infrared. Fourier-transform infrared spectroscopy (FT-IR) was conducted using a Bruker Alpha-P ATR-spectrometer (Bruker AXS, Karlsruhe, Germany) in an attenuated total reflection configuration. The data evaluation was carried out using the OPUS program (Bruker, Ettlingen, Germany).

DSC. Differential scanning calorimetry (DSC) was performed with a computer-controlled PhoenixDSC 204 F1 thermal analyser (Netzsch, Selb, Germany). A thermal ramp of 5 °C min^{-1} was used for the measurements that were carried out from −80 °C to 150 °C under a nitrogen atmosphere supplied by a flow at a rate of 40 mL min^{-1}. Cold-sealed and punctured aluminium pans were used as sample containers. The samples were first cooled to −80 °C. The given temperatures correspond to the onset.

TGA. ThermoGravimetric analyses (TGA) were performed with a TG 449 F3 Jupiter (Netzsch, Selb, Germany). Measurements were carried out in aluminum oxide crucibles with a heating rate of 10 °C min^{-1} and nitrogen as purge gas with a flow rate of 40 mL min^{-1}. The given temperatures correspond to a 5% onset.

Luminescence spectroscopy. Emission and excitation spectra were recorded using a HORIBA Jobin Yvon FluoroLog-3 modular spectrofluorometer with a continuous xenon lamp (450 W) as the excitation source and an R928P PMT detector. A white laser, Fianium WhiteLase, was employed as a source for data acquisition, with the instrument operating in a TCSPC (time-correlated single photon counting) mode.

Synthetic procedures

General procedure for synthesis of potassium tetrakis(8-quinolinato)lanthanidate K[Ln(Q)$_4$]. The potassium tetrakis(8-quinolinato)lanthanidate salts K[Ln(Q)$_4$] (Ln = Dy–Lu and Y) were prepared by modifying a procedure reported for Na[Y(Q57Cl)$_4$] (Q57Cl = 5,7-dichloro-8-quinolinolate).[26] Potassium hydroxide (8.0 mmol, 4.0 eq.) was added to a solution of 8-hydroxyquinoline (8.0 mmol, 4.0 eq.) in ethanol at 70 °C. After stirring for 1 h at 70 °C, an ethanolic solution of the rare earth chloride hexahydrate, $LnCl_3\cdot 6H_2O$, (2.0 mmol, 1.0 eq.) was added. The resulting yellow precipitate was stirred for 24 h at 70 °C, filtered and washed with water and ethanol. By drying the precipitate in air, the tetrakis complexes were obtained as a yellow powder in an almost quantitative yield.

General procedure for the synthesis of tetrabutylphosphonium bromide [P$_{4444}$]Br. A Schlenk flask under argon was introduced to tributylphosphine (P_{444}) (1.0 eq.) and bromobutane (1.0 eq.). The mixture was stirred at 120 °C for 72 hours. Once back at room temperature, the flask was put under a dynamic vacuum to remove all the volatile compounds. $[P_{4444}]Br$ was obtained as a white solid.

General procedure for synthesis of tetrabutylphosphonium tetrakis(8-quinolinato)lanthanidate [P$_{4444}$][Ln(Q)$_4$]·2H$_2$O. For the exchange of potassium with tetrabutylphosphonium, K[Ln(Q)$_4$] (1.0 eq.) was stirred in acetone at room temperature for 1 h. $[P_{4444}]Br$ (1.0 eq.) was added, and the reaction mixture was stirred at room temperature for 3 d. The non-reacted starting materials were filtered, and the solvent was removed in a vacuum. The resulting brown sticky solid was washed with water, filtered, and dried in air. The final product was obtained as a yellow powder.

Tetrabutylphosphonium tetrakis(8-quinolinato)dysprosiate dihydrate [P$_{4444}$][Dy(Q)$_4$]·2H$_2$O. ν_{max} (cm^{-1}): 3308, 3046, 2959, 2930, 2871, 1688, 1598, 1565, 1493, 1458, 1423, 1380, 1368, 1321, 1280, 1226, 1173, 1135, 1105, 1056, 1032, 1000, 961, 904, 860, 823, 790, 742, 727, 651, 603, 556, 499, 485.

Tetrabutylphosphonium tetrakis(8-quinolinato)holmiate dihydrate [P$_{4444}$][Ho(Q)$_4$]·2H$_2$O. ν_{max} (cm^{-1}): 3045, 2958, 2930, 2870, 1597, 1562, 1494, 1459, 1423, 1383, 1365, 1325, 1281, 1262, 1225, 1169, 1134, 1107, 1055, 1032, 1004, 968, 905, 823, 800, 790, 727, 652, 603, 555, 523, 500, 484.

Tetrabutylphosphonium tetrakis(8-quinolinato)erbiate dihydrate [P$_{4444}$][Er(Q)$_4$]·2H$_2$O. ν_{max} (cm^{-1}): 3413, 3041, 2960, 2930, 2871, 1679, 1598, 1566, 1494, 1458, 1425, 1381, 1368, 1321, 1280, 1227, 1171, 1136, 1107, 1057, 1033, 1003, 962, 904, 855, 823, 791, 740, 729, 651, 604, 571, 558, 500, 485, 433.

Tetrabutylphosphonium tetrakis(8-quinolinato)thulliate dihydrate [P$_{4444}$][Tm(Q)$_4$]·2H$_2$O. ν_{max} (cm^{-1}): 3300, 3047, 2959, 2929, 2870, 1686, 1598, 1565, 1493, 1458, 1424, 1381, 1368, 1322, 1281, 1226,

1173, 1135, 1106, 1056, 1032, 1000, 961, 904, 858, 823, 791, 741, 727, 651, 604, 557, 500, 486, 433.

Tetrabutylphosphonium tetrakis(8-quinolinato)lutetiate dihydrate $[P_{4444}][Lu(Q)_4]\cdot 2H_2O$. ^{1}H-NMR (400 MHz, DMSO-d$_6$): 0.91 (t, J_{H-H} = 6.8 Hz, 12H), 1.38–1.45 (m, 16H), 2.11–2.17 (m, 8H), 6.38 (d, J_{H-H} = 8.0 Hz, 4H), 6.59 (d, J_{H-H} = 8.0 Hz, 4H), 7.12 (dd, J_{H-H} = 8.0 Hz, J_{H-H} = 8.0 Hz, 4H), 7.23 (dd, J_{H-H} = 8.0 Hz, J_{H-H} = 4.0 Hz, 4H), 7.97 (d, J_{H-H} = 8.0 Hz, 4H), 8.72 (d, J_{H-H} = 4.0 Hz, 4H). ^{13}C-NMR (100 MHz, DMSO-d$_6$): 13.2, 17.3 (d, J_{P-C} = 47.4 Hz), 22.6 (d, J_{P-C} = 4.9 Hz), 23.3 (d, J_{P-C} = 15.7 Hz), 107.5, 111.4, 120.4, 129.3, 129.8, 136.0, 143.9, 145.6, 166.8. ν_{max} (cm^{-1}): 3304, 3047, 2958, 2930, 2870, 1687, 1598, 1566, 1494, 1458, 1424, 1380, 1369, 1323, 1282, 1226, 1204, 1170, 1107, 1056, 1032, 1000, 983, 964, 905, 868, 824, 790, 729, 652, 604, 558, 500, 488, 440, 421.

Tetrabutylphosphonium tetrakis(8-quinolinato)yttriate dihydrate $[P_{4444}][Y(Q)_4]\cdot 2H_2O$. ^{1}H-NMR (400 MHz, DMSO-d$_6$): 0.91 (t, J_{H-H} = 6.8 Hz, 12H), 1.38–1.42 (m, 16H), 2.12–2.19 (m, 8H), 6.39 (d, J_{H-H} = 8.0 Hz, 4H), 6.63 (d, J_{H-H} = 8.0 Hz, 4H), 7.13 (dd, J_{H-H} = 8.0 Hz, J_{H-H} = 8.0 Hz, 4H), 7.27 (dd, J_{H-H} = 8.0 Hz, J_{H-H} = 4.0 Hz, 4H), 8.02 (d, J_{H-H} = 8.0 Hz, 4H), 8.79 (d, J_{H-H} = 4.0 Hz, 4H). ^{13}C-NMR (100 MHz, DMSO-d$_6$): 13.1, 17.3 (d, J_{P-C} = 47.4 Hz), 22.5 (d, J_{P-C} = 4.9 Hz), 23.2 (d, J_{P-C} = 15.5 Hz), 107.8, 111.4, 120.3, 129.2, 129.7, 136.4, 144.0, 145.8, 166.3. ν_{max} (cm^{-1}): 3045, 2958, 2929, 2870, 1687, 1597, 1562, 1494, 1459, 1423, 1381, 1365, 1321, 1279, 1224, 1204, 1170, 1134, 1106, 1055, 1032, 1003, 964, 904, 855, 822, 788, 727, 652, 603, 568, 499, 484, 435.

Conclusions

$[P_{4444}][Ln(Q)_4]\cdot 2X$ (Ln = Dy–Lu and Y; Q = 8-quinolinolato; X = H_2O for Ln = Dy–Tm, Lu and Y and $(CH_3)_2CO$ for Ln = Yb) was synthesized by a metathesis reaction of the respective potassium tetrakis(8-quinolinolato)lanthanidate salts with tetrabutylphosphonium bromide in acetone at room temperature. Single X-ray structure analysis shows that $[P_{4444}][Ln(Q)_4]\cdot 2H_2O$ (Ln = Dy–Lu and Y) crystallizes isostructurally. They, as well as $[P_{4444}][Yb(Q)_4]\cdot 2(CH_3)_2CO$, feature two solvent molecules (water or acetone) that are present in the structure but are not coordinated to the metal. The solvent is lost upon heating, as thermal analyses reveal. Luminescence studies reveal that all compounds are green emitters with short lifetimes in the ns range. Depending on the lanthanide ion, the luminescence colour varies between yellow-green and blue-green. Thus, this series of lanthanide materials demonstrates that luminescence colour tuning is not only possible through tuning of the electronic structure of the ligand as commonly employed[32] but also through the subtle change in metal–ligand interactions along the series of lanthanides.

Conflicts of interest

There are no conflicts to declare.

Data availability

All other data supporting this article have been included as part of the SI. Supplementary information available: ^{1}H-, ^{13}C- and ^{31}P-NMR and FTIR spectra, PXRD patterns, thermal data and luminescence analysis. See DOI: **https://doi.org/10.1039/d4nj03697b**

Crystallographic data have been deposited at the CCDC under 2126657–2126663.[44–50]

Acknowledgements

A.-V. M. would like to thank the Royal Academy of Sciences, Sweden, for support through the Göran Gustafsson prize in Chemistry, Energimyndigheten (Swedish Energy Agency) for support through grant no. 46676-1 and Vetenskapsrådet for support through grant no. 2019-02345 and 2020-04437. A.-V. M. acknowledges support to GB from the SSF-funded REFIT project and to VR through project no. 2020-04437. The Novonordisk foundation is acknowledged for support with a RECRUIT grant for A.-V. M. A.-V. M. is indebted to the Villum Foundation for a Villum Investigator award.

Notes and references

1 J. Zhou, Q. Liu, W. Feng, Y. Sun and F. Li, *Chem. Rev.*, 2015, **115**, 395.
2 C. Chen and J. Shi, *Coord. Chem. Rev.*, 1998, **171**, 161.
3 C. W. Tang and S. A. VanSlyke, *Appl. Phys. Lett.*, 1987, **51**, 913.
4 M. Cölle, R. E. Dinnebier and W. Brütting, *Chem. Commun.*, 2002, 2908.
5 X. Sun, D.-Y. Zhou, L. Qiu, L.-S. Liao and F. Yan, *J. Phys. Chem. C*, 2011, **115**, 2433.
6 C. F. R. A. C. Lima, R. J. S. Taveira, J. C. S. Costa, A. M. Fernandes, A. Melo, A. M. S. Silva and L. M. N. B. F. Santos, *Phys. Chem. Chem. Phys.*, 2016, **18**, 16555.
7 Z. Shahedi, M. R. Jafari and A. A. Zolanvari, *J. Mater. Sci.: Mater. Electron.*, 2017, **28**, 7313.
8 M. Goldman and E. L. Wehry, *Anal. Chem.*, 1970, **42**, 1178.
9 B. Adranno, O. Renier, G. Bousrez, V. Paterlini, G. V. Baryshnikov, V. Smetana, S. Tang, H. Ågren, A. Metlen, L. Edman and A.-V. Mudring, *Adv. Photon. Res.*, 2023, **4**, 2200279.
10 R. J. Curry and W. P. Gillin, *Appl. Phys. Lett.*, 1999, **75**, 1380.
11 W. P. Gillin and R. J. Curry, *Appl. Phys. Lett.*, 1999, **74**, 798.
12 E. V. Baranov, G. K. Fukin, T. V. Balashova, A. P. Pushkarev, I. D. Grishin and M. N. Bochkarev, *Dalton Trans.*, 2013, **42**, 15699.
13 S. G. Leary, G. B. Deacon and P. C. Junk, *Z. Anorg. Allg. Chem.*, 2005, **631**, 2647.
14 S. W. Magennis, A. J. Ferguson, T. Bryden, T. S. Jones, A. Beeby and I. D. W. Samuel, *Synth. Met.*, 2003, **138**, 463.
15 F. Artizzu, L. Marchiò, M. L. Mercuri, L. Pilia, A. Serpe, F. Quochi, R. Orrù, F. Cordella, M. Saba, A. Mura, G. Bongiovanni and P. Deplano, *Adv. Funct. Mater.*, 2007, **17**, 2365.
16 F. Artizzu, F. Quochi, L. Marchiò, R. F. Correia, M. Saba, A. Serpe, A. Mura, M. L. Mercuri, G. Bongiovanni and P. Deplano, *Chem. – Eur. J.*, 2015, **21**, 3882.

17 N. F. Chilton, G. B. Deacon, O. Gazukin, P. C. Junk, B. Kersting, S. K. Langley, B. Moubaraki, K. S. Murray, F. Schleife, M. Shome, D. R. Turner and J. A. Walker, *Inorg. Chem.*, 2014, **53**, 2528.
18 O. Khreis, R. Curry, M. Somerton and W. P. Gillin, *J. Appl. Phys.*, 2000, **88**, 777.
19 S. Penna, A. Reale, R. Pizzoferrato, G. Tosi Beleffi, D. Musella and W. Gillin, *Appl. Phys. Lett.*, 2007, **91**, 021106.
20 O. Khreis, W. P. Gillin, M. Somerton and R. Curry, *Org. Electron.*, 2001, **2**, 45.
21 R. Van Deun, P. Fias, K. Driesen, K. Binnemans and C. Görller-Walrand, *Phys. Chem. Chem. Phys.*, 2003, **5**, 2754.
22 G. B. Deacon, T. Dierkes, M. Hübner, P. C. Junk, Y. Lorenz and A. Urbatsch, *Eur. J. Inorg. Chem.*, 2011, 4338.
23 K. Tsunashima and M. Sugiya, *Electrochem. Commun.*, 2007, **9**, 2353.
24 K. Tsunashima and M. Sugiya, *Electrochemistry*, 2007, **75**, 734.
25 K. J. Fraser and D. R. MacFarlane, *Aust. J. Chem.*, 2009, **62**, 309.
26 R. Van Deun, P. Fias, P. Nockemann, A. Schepers, T. N. Parac-Vogt, K. Van Hecke, L. Van Meervelt and K. Binnemans, *Inorg. Chem.*, 2004, **43**, 8461.
27 M. Melegari, M. Neri, A. Falco, M. Tegoni, M. Maffini, F. Fornari, C. Mucchino, F. Artizzu, A. Serpe and L. Marcio, *ChemSusChem*, 2024, **17**, e202400286.
28 R. D. Shannon, *Acta Crystallogr., Sect. A*, 1976, **32**, 751.
29 R. Wang, Y. Cao, D. Jia, L. Liu and F. Li, *Opt. Mater.*, 2013, **36**, 232.
30 B. Yan and K. Sheng, *Synth. Met.*, 2010, **160**, 1449.
31 P. J. Han, A. L. Rheingold and W. C. Trogler, *Inorg. Chem.*, 2013, **52**, 12033.
32 W. Humbs, E. van Veldhoven, H. Zhang and M. Glasbeek, *Chem. Phys. Lett.*, 1999, **304**, 10.
33 M. Ottonelli, G. M. M. Izzo, F. Rizzo, G. Musso, G. Dellepiane and R. Tubino, *J. Phys. Chem. B*, 2005, **109**, 19249.
34 C. Zhong, Q. Wu, R. Guo and H. Zhang, *Opt. Mater.*, 2008, **30**, 870.
35 C. H. Chen and J. Shi, *Coord. Chem. Rev.*, 1998, **171**, 161.
36 G. H. Dieke, H. M. Crosswhite and H. Crosswhite, *Spectra and energy levels of rare earth ions in crystals*, 1968.
37 T. Tsuboi, K. H. Jang, S. Polosan, K. Shimamura, M. Bettinelli and H. J. Seo, *J. Lumin.*, 2011, **131**, 695.
38 G. M. Sheldrick, *Acta Crystallogr., Sect. A: Found. Adv.*, 2015, **71**, 3.
39 G. M. Sheldrick, *Acta Crystallogr., Sect. C: Struct, Chem.*, 2015, **71**, 3.
40 *B. A. I. SAINT*, Bruker AXS Inc., Madison, Wisconsin, USA, 2015.
41 M. Bruker, *APEX3 and SADABS*. Bruker AXS Inc., Wisconsin, USA, 2016.
42 K. Brandenburg and H. Putz, *DIAMOND: Program for Crystal and Molecular Structure Visualization*, Crystal Impact GbR, Bonn, Germany, 2011.
43 C. F. Macrae, P. R. Edgington, P. McCabe, E. Pidcock, G. P. Shields, R. Taylor, M. Towler and J. Streek, *J. Appl. Crystallogr.*, 2006, **39**, 453.
44 S. Kammereck, G. Bousrez, O. Renier, V. Paterlini, V. Smetana and A.-V. Mudring, CCDC 2126657: Experimental Crystal Structure Determination, 2025, DOI: **10.5517/ccdc.csd.cc29cyvh**.
45 S. Kammereck, G. Bousrez, O. Renier, V. Paterlini, V. Smetana and A.-V. Mudring, CCDC 2126658: Experimental Crystal Structure Determination, 2025, DOI: **10.5517/ccdc.csd.cc29cywj**.
46 S. Kammereck, G. Bousrez, O. Renier, V. Paterlini, V. Smetana and A.-V. Mudring, CCDC 2126659: Experimental Crystal Structure Determination, 2025, DOI: **10.5517/ccdc.csd.cc29cyxk**.
47 S. Kammereck, G. Bousrez, O. Renier, V. Paterlini, V. Smetana and A.-V. Mudring, CCDC 2126660: Experimental Crystal Structure Determination, 2025, DOI: **10.5517/ccdc.csd.cc29cyyl**.
48 S. Kammereck, G. Bousrez, O. Renier, V. Paterlini, V. Smetana and A.-V. Mudring, CCDC 2126661: Experimental Crystal Structure Determination, 2025, DOI: **10.5517/ccdc.csd.cc29cyzm**.
49 S. Kammereck, G. Bousrez, O. Renier, V. Paterlini, V. Smetana and A.-V. Mudring, 2025, CCDC 2126662: Experimental Crystal Structure Determination, 2025, DOI: **10.5517/ccdc.csd.cc29cz0p**.
50 S. Kammereck, G. Bousrez, O. Renier, V. Paterlini, V. Smetana and A.-V. Mudring, CCDC 2126663: Experimental Crystal Structure Determination, 2025, DOI: **10.5517/ccdc.csd.cc29cz1q**.

